Importance of many-body correlations in glass transition: An example from polydisperse hard spheres

Mathieu Leocmach, John Russo, Hajime Tanaka

AIP | The Journal of Chemical Physics

Importance of many-body correlations in glass transition: An example from polydisperse hard spheres

Mathieu Leocmach, John Russo, and Hajime Tanaka

Citation: J. Chem. Phys. **138**, 12A536 (2013); doi: 10.1063/1.4769981
View online: http://dx.doi.org/10.1063/1.4769981
View Table of Contents: http://jcp.aip.org/resource/1/JCPSA6/v138/i12
Published by the American Institute of Physics.

Importance of many-body correlations in glass transition: An example from polydisperse hard spheres

Mathieu Leocmach,[a),b)] John Russo,[b),c)] and Hajime Tanaka[d)]
Institute of Industrial Science, University of Tokyo, 4-6-1 Komaba, Meguro-ku, Tokyo 153-8505, Japan

(Received 12 October 2012; accepted 20 November 2012; published online 14 February 2013)

Most of the liquid-state theories, including glass-transition theories, are constructed on the basis of two-body density correlations. However, we have recently shown that many-body correlations, in particular, bond orientational correlations, play a key role in both the glass transition and the crystallization transition. Here we show, with numerical simulations of supercooled polydisperse hard spheres systems, that the length-scale associated with any two-point spatial correlation function does not increase toward the glass transition. A growing length-scale is instead revealed by considering many-body correlation functions, such as correlators of orientational order, which follows the length-scale of the dynamic heterogeneities. Despite the growing of crystal-like bond orientational order, we reveal that the stability against crystallization with increasing polydispersity is due to an increasing population of icosahedral arrangements of particles. Our results suggest that, for this type of systems, many-body correlations are a manifestation of the link between the vitrification and the crystallization phenomena. Whether a system is vitrified or crystallized can be controlled by the degree of frustration against crystallization, polydispersity in this case. © *2013 American Institute of Physics*. [http://dx.doi.org/10.1063/1.4769981]

I. INTRODUCTION

Amorphous materials have been of prime importance in our technology for millennia, from antique glass works to fashionable phones made of metallic glass. One of the new frontiers of the amorphous technology is in the design of amorphous drugs,[1,2] better absorbed by our metabolism with less side effects, that would be stable at room temperature. The main obstacle is a lack of our basic understanding of the physics of the glass transition, without any operative consensus despite half a century of intensive research.[3,4]

When cooled below its freezing temperature while avoiding crystallization, a liquid becomes supercooled. Upon further cooling, the dynamics slows down by many orders of magnitude leading to a material that is mechanically a solid without long range positional order, thus called amorphous. It is now known that the dynamics in a supercooled liquid is heterogeneous, with a length-scale that grows when approaching the glass transition[5,6] (see Ref. 4 for a review). The length-scale defined by the dynamical heterogeneity is not static (one-time spatial correlation) but dynamic (two-time spatial correlation).

The existence of a static (structural) length that would grow and accompany the dynamic heterogeneities is still not clear in the general case. However, in a class of system that includes polydisperse hard spheres, we have shown[7] that some medium range bond orientational order reminiscent of the crystal exists in the supercooled liquid and grows toward the glass transition in the same way as the dynamical heterogeneity. The presence in glassy materials of structures locally reminiscent of crystals has been confirmed recently in amorphous silicon[8] and in a metallic glass.[9] While bond orientational order is a member of the class of many-body correlations between neighboring particles, it is yet unclear if a similar length-scale can be extracted from two-body correlation functions. This question is particularly important considering that the mode-coupling theory (MCT) of the glass transition takes as input only two-body quantities, and similarly, modern spin-glass-type theories of the structural glass transition[10–12] are not taking explicitly into account many-body correlations.

At polydispersities over 6%–7%, the system needs to fractionate to crystallize.[13] What is the bond order of the reference crystal is then unclear and may challenge our scenario. This is a situation reminiscent of binary hard sphere systems of size ratio close to one[14,15] where growing bond order has not been reported.[16] However, it is known that even in binary systems locally favored structures play a role in the slowing down of the dynamics in some cases.[17,18] Interestingly, recent studies by Mosayebi *et al.*[19,20] demonstrate that there are static growing lengths in binary Lennard-Jones and soft sphere mixtures. They estimated the static length by looking at the spatial correlation of the degree of non-affine deformation of inherent structures under shear deformation.

In the present study we will use polydisperse hard sphere systems, where we know how to extract meaningful many-body correlations, and look for a two-body quantity that would show the same behavior as the bond order. We will show that the two-body part of the free energy (which, for hard potentials, correspond to the two-body part of the structural entropy) is unable to capture medium range bond

a)Electronic mail: mathieu.leocmach@polytechnique.org. Present address: Laboratoire de Physique, CNRS UMR 5672, Ecole Normale Suprieure de Lyon, 46 alle d'Italie, 69364 Lyon cedex 07, France.
b)M. Leocmach and J. Russo contributed equally to this work.
c)Electronic mail: russoj@iis.u-tokyo.ac.jp.
d)Electronic mail: tanaka@iis.u-tokyo.ac.jp.

ordered regions or to yield correlation lengths meaningful from the point of view of the glass transition. We thus confirm the medium range crystalline order scenario and test its robustness against increasing polydispersity. Since bond orientational order is directly linked to the underlying crystalline structures, we will then address the important question of what is the mechanism responsible for the avoidance of crystallization. We will show that in the metastable fluid phase, crystalline packings are in competition with icosahedral packings, and that polydispersity acts in favor of the latter ones.

The paper is organized as follows. In Sec. II, we present the details of the simulations and the order parameters considered in this work. In Sec. III, the results are organized into a study of the order parameters distribution (Sec. III A) and their static length-scales (Sec. III B), and a method to determine the competition between crystalline structures and icosahedral packings (Sec. III C). In Sec. IV, we discuss our results. In Sec. V, we summarize our work.

II. METHODS

A. Simulation method

We run Monte Carlo simulations in the isothermal-isobaric ensemble (NpT) for $N = 4000$ polydisperse hard spheres. The diameters (σ) follow a Gaussian distribution $P(\sigma) = \exp[-(\sigma - \sigma_0)^2/2s^2]/\sqrt{2\pi}s$, with polydispersity index $\Delta = s/\sigma_0$. In the following, we fix the unit of length as $\sigma_0 = 1$ and the unit of energy so that the Boltzmann constant is unity, $k_B = 1$.

B. Estimation of two-point quantities: Pair entropy and pair free energy

Our aim is to compare the behavior of both two-point quantities and many-body quantities with increasing pressure. Due to the hard-sphere interaction, entropy is the only contribution to the system free energy. All two-pair correlation quantities are thus derived from the two-body excess entropy,[21,22] defined as

$$s_2 = -\frac{\rho k_B}{2}\int dr[g(r)\log(g(r)) - g(r) + 1]. \quad (1)$$

In principle, s_2 can be calculated separately for each particle i in the system. In practice, this requires time averages to compute the pair correlation function of each particle, $g_i(r)$, where the particle distribution around a particle i is averaged over short-time scales (β processes). In Refs. 7, 23, and 24 we averaged on times comparable or longer than the α relaxation, leading to a quantity that was trivially a reflection of the dynamical heterogeneity.

Here we instead construct an approximate but instantaneous $s_2(i)$ using the pair correlation function $g(r)$:

$$s_2(i) = -\frac{\rho k_B}{2}\sum_j [g(r_{ij})\log(g(r_{ij})) - g(r_{ij}) + 1]. \quad (2)$$

This quantity is in very good agreement with the one obtained by calculating the radial distribution function for each particle, $g_i(r)$, averaged over times comparable to the β relaxation time.

More rigorously, one can compute directly the free-energy of each configuration by measuring the free volume of the particles, defined as the volume ($v(i)$) in which each sphere can freely move while holding all the other spheres fixed. It has been shown[25] that this free volume is simply related to the pair free-energy (f_2) by the following relation:

$$f_2 = \sum_i f_2(i) = -k_B T \sum_i \log(v(i)/\lambda), \quad (3)$$

where λ is the thermal de Broglie wavelength. To compute the free volume $v(i)$, we follow previous studies:[25] first the Voronoi-diagram for each configuration is computed, and the polyhedron surrounding each particle is determined. To account for polydispersity, we employ the radical Voronoi tessellation. The free volume of particle i is then computed by shifting normally all the faces of the corresponding polyhedron by $\sigma(i)/2$ toward particle i, and computing the new volume. In this way the volume $v(i)$ represents the volume in which the excluded volume of particle i can move without leaving its Voronoi cell. This procedure is conducted independently for each particle and for each configuration.

C. Estimation of many-point quantities: Bond orientational order parameter analysis

To study many-body correlations we use the local bond-order analysis introduced by Steinhardt,[26] first applied to study crystal nucleation by Frenkel and co-workers.[27] The ℓ-fold symmetry of a neighborhood around each particle i is characterized by a $(2\ell + 1)$ dimensional complex vector $(\mathbf{q}_l)$ as $q_{\ell m}(i) = \frac{1}{N_b(i)}\sum_{j=1}^{N_b(i)} Y_{\ell m}(\hat{\mathbf{r}}_{\mathbf{ij}})$, where ℓ is a free integer parameter, and m is an integer that runs from $m = -\ell$ to $m = \ell$. The functions $Y_{\ell m}$ are the spherical harmonics and $\hat{\mathbf{r}}_{\mathbf{ij}}$ is the vector from particle i to particle j. The sum goes over all neighboring particles $N_b(i)$ of particle i. Usually $N_b(i)$ is defined by all particles within a cutoff distance, but in an inhomogeneous system the cutoff distance would have to change according to the local density. Instead, we sort neighbors according to their distances from particle i, and fix $N_b(i) = 12$ which is the number of nearest neighbors in icosahedra and close packed crystals (like hcp and fcc) which are known to be the only relevant crystalline structures for hard spheres.

In the analysis, one uses the rotational invariants defined as

$$q_\ell = \sqrt{\frac{4\pi}{2l+1}\sum_{m=-\ell}^{\ell} |q_{\ell m}|^2}, \quad (4)$$

$$w_\ell = \sum_{m_1+m_2+m_3=0} \begin{pmatrix} \ell & \ell & \ell \\ m_1 & m_2 & m_3 \end{pmatrix} q_{\ell m_1} q_{\ell m_2} q_{\ell m_3}, \quad (5)$$

where the term in brackets in Eq. (5) is the Wigner 3-j symbol. In particular, both crystalline and icosahedral neighborhoods have high q_6 (strong 6-fold symmetry), with the highest values for the latter. To detect specifically icosahedral order, one prefers w_6, whose minimum value is obtained only by a perfect icosahedron.

The identification of crystalline particles follows the usual procedure.[27] A particle is identified as crystal if its orientational order is coherent (in symmetry and in orientation) with that of its neighbors. The scalar product $(\mathbf{q}_6(i)/|\mathbf{q}_6(i)|) \cdot (\mathbf{q}_6(j)/|\mathbf{q}_6(j)|)$ quantifies this similarity. If it exceeds 0.7 between two neighbors, they are deemed *connected*. We then identify a particle as crystalline if it is connected with at least 7 neighbors.[27] In a more continuous way, summing the contribution of all the bonds of a given particle, we define the "crystallinity:"[28]

$$\mathrm{C}(i) = \sum_{j=0}^{N_b(i)} \frac{\mathbf{q}_6(i) \cdot \mathbf{q}_6(j)}{|\mathbf{q}_6(i)|\,|\mathbf{q}_6(j)|}. \tag{6}$$

Alternatively, one can coarse-grain $\mathbf{q}_\ell$ over the neighbors,[29]

$$Q_{\ell m}(i) = \frac{1}{N(i)+1}\left(q_{\ell m}(i) + \sum_{j=0}^{N(i)} q_{\ell m}(j)\right), \tag{7}$$

to suppress the signal from locally incoherent orientations (icosahedral order)[30] and use the resulting invariant Q_6 as an indication of crystallinity, more precisely, the degree of crystal-like rotational symmetry. Alternatively, we note that the shortcomings of non-coarse-grained order parameters in the identification of crystallinity can be addressed by Minkowski tensors.[31]

Here, we briefly consider the physical meaning of crystal-like bond orientational order parameters. The crystallization transition is characterized by the symmetry breaking of both orientational and translational order. We note that both C and Q_6 are good measures of bond orientational order, whereas the density or other two-body quantities are measures of translational order. It was shown[28] that in hard spheres crystallization is driven by fluctuations in bond orientational order and not by density fluctuations. Crystals continuously form, grow, and melt in regions of high bond orientational order, which then effectively act as precursors for the crystallization transition. So C and Q_6, while not being direct indicators for the presence of crystals, rather measure the tendency to promote crystallization. In Sec. III B we are going to show that indeed the length-scale associated with bond orientational order fluctuations increases with supercooling. Then in Sec. III C we are going to study the mechanism by which the crystallization transition is avoided.

D. Estimation of the correlation lengths of various quantities

Finally, we explain how to evaluate the correlation length of various order parameters. The calculation can be carried out both in real space and in Fourier space. While formally containing the same information, the Fourier analysis has some practical advantages over the real space analysis. In real space, the correlation function of any order parameter is an oscillating and rapidly decaying function of r. The correlation length is obtained by fitting the *envelope* of the correlation function with an Ornstein-Zernike expression. This expression is only asymptotic, so the two first peaks at short r should be omitted, and it is also rapidly decaying, so that the statistical noise strongly affects the quality of the fit at long r. The problem is less severe for order parameters having a tensorial nature, and correlation lengths of crystal-like bond orientational order have been easily measured in real space in previous studies.[7,28,30,32,33] For example, the tensorial order parameter Q_{6m} effectively correlates 7 scalar fields, allowing a sevenfold reduction of the noise. But the real space analysis requires much longer time averages for two-body correlation functions, both f_2 and s_2, which have a purely scalar nature. This problem can be overcome by calculating the correlation functions in Fourier space. These functions are not oscillatory at small q where we can expect the Ornstein-Zernike form, and thus much easier to fit unambiguously. So, to keep both two-body and many-body correlation functions consistent, we calculate all correlations in Fourier space. We explain in the following a straightforward procedure to extract correlation length from Fourier space analysis.

At a given time step, for any scalar order parameter field x increasing with order, we compute a structure factor keeping only the 10% most ordered particles (more on this choice below). This condition defines a threshold x^*. The ensemble average of the thresholds $\langle x^* \rangle$ are indicated in Fig. 2. Formally, we define a function $\omega(i) = \Theta[x(i) - x^*]$, where $\Theta(x)$ is the Heaviside's step function, and a four-point structure factor,

$$S_x(q) = N^{-1}(\langle \Omega(\mathbf{q})\Omega(-\mathbf{q})\rangle - |\,\langle \Omega(\mathbf{q})\rangle^2\,|), \tag{8}$$

where $\Omega(\mathbf{q})$ is the Fourier transform of $\omega(i)$:

$$\Omega(\mathbf{q}) = \sum_i \omega(i) \exp(-\imath\,\mathbf{q}\cdot\mathbf{r}_i). \tag{9}$$

This structure factor is then ensemble averaged (still noted $S_x(q)$ for concision) over $\approx 10^4$ configurations. The case of order parameters decreasing toward ordering (i.e., s_2, w_6) is trivially obtained by changing the sign.

III. RESULTS

Figure 1 shows the equation of state for the simulated state points. In particular, we consider three data-sets. The first one (blue filled circles in the figure) corresponds to simulations at a constant polydispersity of $\Delta = 7\%$. For each

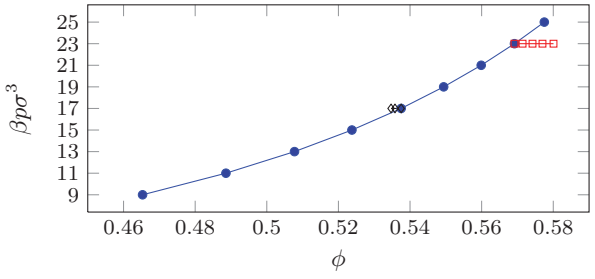

FIG. 1. Simulated state points. The blue filled circles (with blue curve) represent the equation of state for polydispersity, $\Delta = 7\%$. The red open squares (with red line) instead are simulation points at the same pressure ($\beta p\sigma^3 = 23$) but at different polydispersities, Δ: from low to high volume fraction they correspond to $\Delta = 7\%$, 9%, 11%, 13%, and 15%, respectively. Similarly, the black open diamonds (with black line) are at $\beta p\sigma^3 = 17$ and $\Delta = 0\%$, 4%, and 7%.

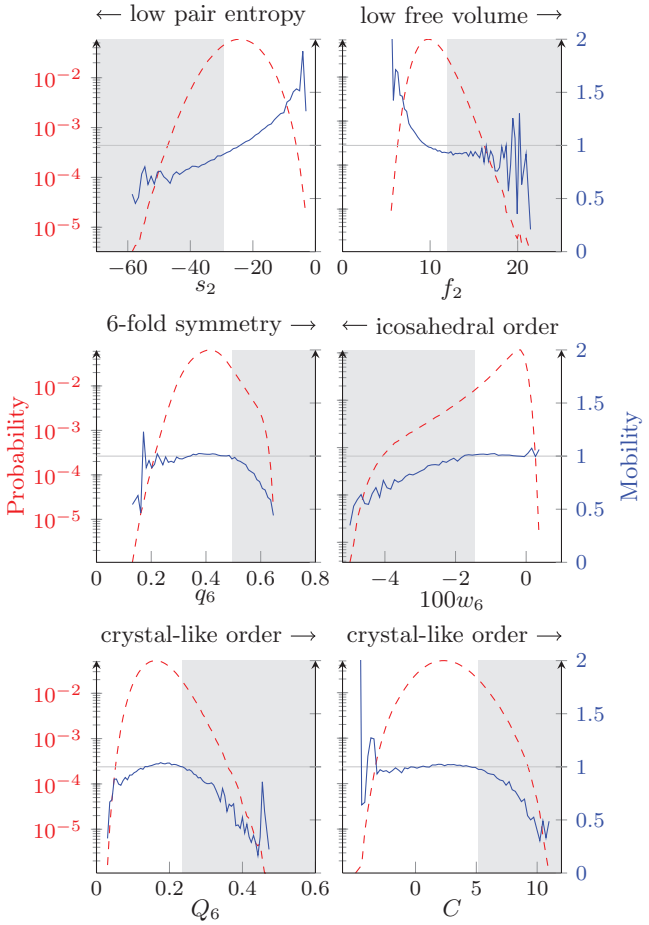

FIG. 2. Probability distributions (red dashed line) and mobility (blue continuous line) function of various order parameters at $\beta p\sigma^3 = 25$ and for a time difference corresponding to the α-relaxation. (Top row): Two-body excess entropy s_2 (left) and pair free energy f_2 (right). (Central row): Local sixfold orientational orders q_6 (left) and w_6 (right). (Bottom row): Coarse-grained Q_6 (left) and crystallinity C (right). Mobility is in unit of mean-square displacement. The shaded area shows the contribution from 10% of the particles having highest (for f_2, q_6, Q_6, and C) or lowest (for s_2, w_6) value of the order parameter.

state point we run 8 independent simulation runs and extract configurations for the calculation of correlation lengths. The second data set (red open squares in the figure) is instead isobaric simulation (at $\beta p\sigma^3 = 23$) with increasing polydispersity, $\Delta = 7\%$, 9%, 11%, 13%, and 15%. The third data set (black open diamonds in the figure) is also isobaric simulation at $\beta p\sigma^3 = 17$ with increasing polydispersity, $\Delta = 0\%$, 4%, and 7%. The two last data sets are used to study the mechanism by which crystallization is suppressed upon an increase of polydispersity, unveiling the role played by icosahedral arrangement of particles.

A. Order parameter distribution and mobility

We study systematically two-body (s_2, f_2) and many-body (q_6, w_6, Q_6, C) scalar order parameter fields for our highest pressure ($\beta p\sigma^3 = 25$). For each of these parameters one can define if a particle is "ordered" or not. Very negative values of s_2 indicate low two-body configurational entropy and thus *a priori* some kind of ordering or stability. Similarly,

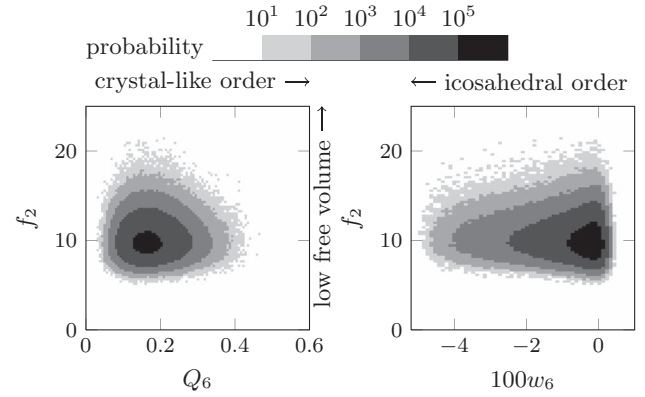

FIG. 3. Correlation between two-body and many-body parameters. Probability distribution functions in the f_2-Q_6 map (left) and in the f_2-w_6 map (right) for a metastable fluid with polydispersity $\Delta = 7\%$ and pressure $\beta p\sigma^3 = 23$. There is no linear correlation between the parameters, meaning that high values of Q_6 (the crystalline regions) or low values of w_6 (the icosahedral regions) are not extremum values of f_2.

high values of f_2 indicate high two-body free energy (low free volume). High values of Q_6 or C indicate locally crystalline environment (locally similar to hcp or fcc crystal), whereas very negative values of w_6 correspond to icosahedral packings. High values of q_6 can indicate ambiguously either crystalline or icosahedral environments.

In Fig. 2 we show the "ordered" side of each parameter as a shaded area, and the probability distribution of this parameter as a red dashed line. Note that for any parameter, the maximum probability does not correspond to the ordered side. However, the probability distribution decays more slowly on the ordered side, indicating the presence of rare but very ordered particles.

By plotting the probability distribution function of the metastable fluid in the (Q_6, f_2) and (w_6, f_2) planes, Fig. 3 shows the absence of linear correlations between f_2 and both Q_6 and w_6. Since Q_6 identifies regions of high crystal-like bond orientational order and w_6 locates icosahedral arrangements of particles, it is clear that high f_2 regions are not associated with any of these structures. We checked in the same way that s_2 is not correlated with many-body parameters.

The absence of strong correlations between two-body quantities and both crystalline and icosahedral packings are also evident from the microscopic dynamics. To study the correlation between any scalar order parameter x and the displacement of the particles, we define the mobility,

$$\Delta r^2(x = x_0, t) \equiv \left\langle \frac{\sum_i \|\mathbf{r}_i(t) - \mathbf{r}_i(0)\|^2 \, \delta(x(i) - x_0)}{\sum_i \delta(x(i) - x_0)} \right\rangle, \tag{10}$$

shown in Fig. 2 for a time difference corresponding to the α-relaxation time. Note that we use δ functions of a constant finite width and thus the number of particles involved in the average of Eq. (10) varies like the probability distribution, explaining the noise in the low probability regions.

We found that for each parameter, its mobility decreases with increasing order. The mobilities of bond-order quantities are flat in the disordered regions and decrease when approaching the perfect structure (i.e., icosahedron for w_6,

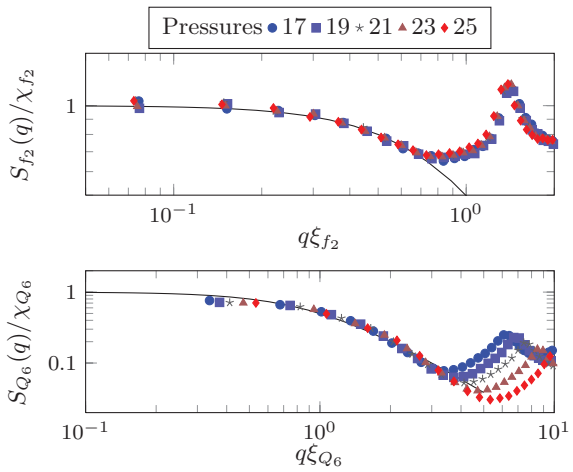

FIG. 4. Structure factors collapse on the Ornstein-Zernike form for (top) f_2 and (bottom) Q_6. Note that the f_2 structure factors are almost similar for all pressures considered. For Q_6 instead, the growth of the correlation length is evident already from the systematic change in the relative position of the nearest-neighbors peaks.

crystal structures for Q_6 or C). By contrast, the mobility of two-body order parameters tends to increase strongly in the disordered region and decreases less in the ordered region (it is almost flat at high f_2). We conclude that many-body quantities describe better the slowing down accompanying good local ordering, while two-body quantities are not clearly correlated to such slower structures. Note that in Fig. 2 both icosahedral packings (low w_6 particles) and bond-ordered crystalline regions (high Q_6 and C) are associated with slow dynamics. As was shown by some of us,[30] the structures primarily responsible for the slowing down of the dynamics are the crystal-like particles, while icosahedral particles act to prevent the crystal nucleation process.[28] This will be shown in detail in Sec. III C.

B. Length-scales

As explained in Sec. II D, we estimate the correlation lengths of various quantities x in Fourier space not only for the two-body s_2 and f_2, but also for scalars derived from the multi-body bond orientational order, i.e., q_6, w_6, Q_6, and C, which allows us to have overall coherency of the length-scale analysis of all the parameters.

Figure 4 shows the increase of $S_x(q)$ toward small wavenumbers ($x = f_2$ upper panel; $x = Q_6$ lower panel), which is well described by the asymptotic Ornstein-Zernike function in Fourier space:

$$S_x(q \to 0) \approx \frac{\chi_x}{1 + \xi_x^2 q^2}, \tag{11}$$

where ξ_x is the correlation length and χ_x the susceptibility of fluctuations of quantity x. In general, an independent determination of χ_x is crucial for the fit.[34] However, here we deal with correlation lengths much smaller than the simulation box and both ξ_x and χ_x can be reliably estimated from a two parameter fit of $S_x(q)$. We note that the absence of the finite-size effects was confirmed for this situation.[7]

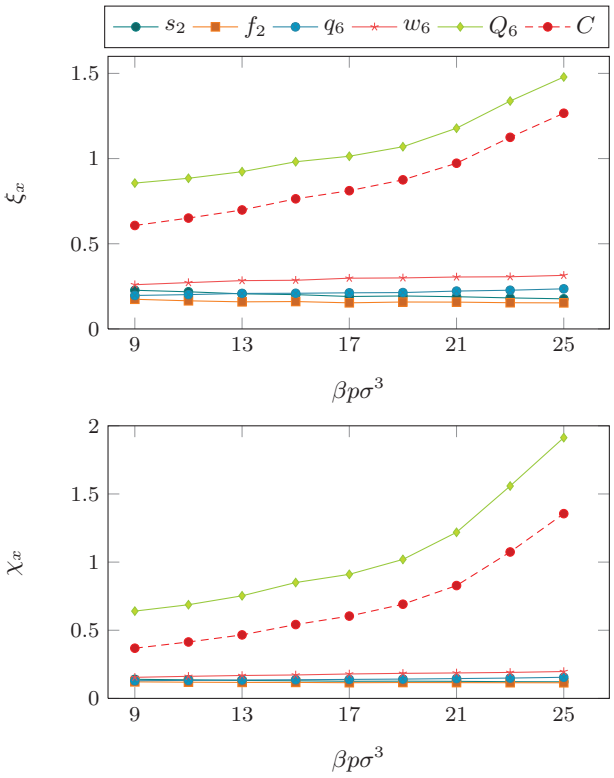

FIG. 5. Correlation length (ξ_x) and susceptibilities (χ_x) extracted for two-body and many-body scalar order parameters, plotted as a function of the pressure. Only many-body correlation lengths are increasing (only slightly for ξ_{w_6}), while the length-scale associated with the two-body quantities is almost constant.

The dependence on the pressure of the resulting correlation lengths ξ_x is shown in Fig. 5. Most of the order parameters produce constant length-scales, including not only the two-body quantities but also q_6, w_6 that are sensible to icosahedral order. The only growing lengths are extracted from measures of local crystal-like order, i.e., Q_6 and C. We confirm that the same results are obtained from real-space correlation functions (but in real space it is possible to detect the growth also in tensorial q_6, see Ref. 35).

The absence of correlations for two-body quantities and the presence of a growing length-scale for Q_6 and C are evident also by direct inspection of the particle configurations. Figure 6 plots the 10% most ordered particles for the different order parameters at $\beta p\sigma^3 = 23$ and $\Delta = 7\%$. The first row of Fig. 6 shows the absence of any appreciable correlation for both two-body quantities f_2 and s_2. The middle row shows that also the signal from icosahedral clusters (both q_6 and w_6 have icosahedra as their extremum) display no appreciable correlation length, i.e., they form randomly and homogeneously throughout the system. Only Q_6 and C (last row in Fig. 6) show clustering of the ordered particles on medium range.

The length-scales obtained from Q_6 or C in Fourier space and from the tensorial $\mathbf{q}_6$ or $\mathbf{Q}_6$ in real space (not shown) are similar and increase monotonically with pressure. Note that the scalar q_6 (dominated by the icosahedral order) yields a very different correlation length. This is consistent with the spatial coherency (in orientation) of crystal-like order that is missing in icosahedral order.[7,30] Coherently, real-space

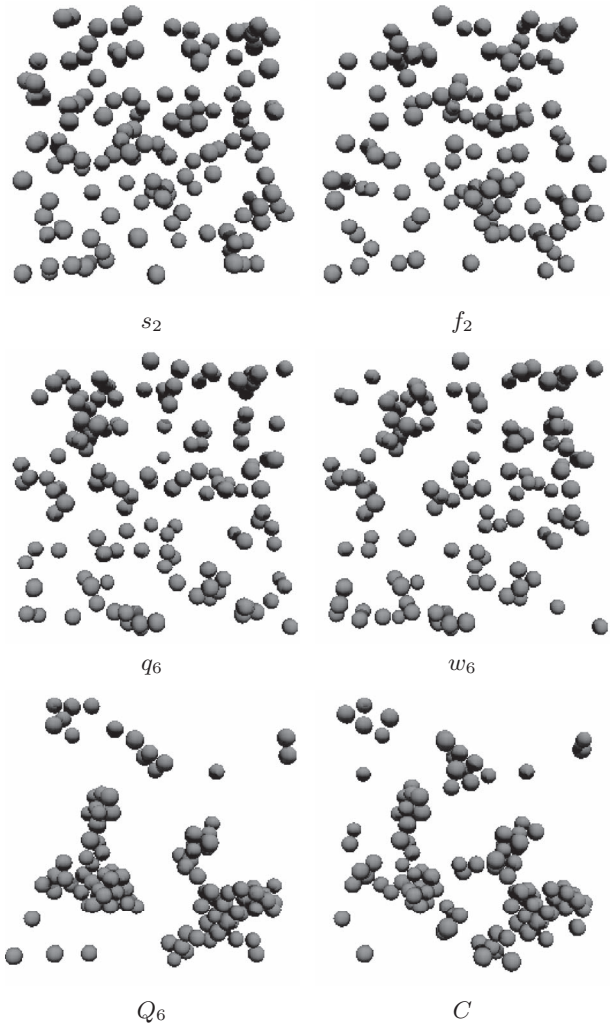

FIG. 6. Visualization of the 10% most ordered particles defined by the various order parameters. All pictures correspond to a thin slice (5σ) of the same configuration at $\beta p\sigma^3 = 23$ and $\Delta = 7\%$. Only Q_6 and C show meaningful spatial fluctuations. We can also see anti-correlation between (Q_6,C) and (q_6,w_6).

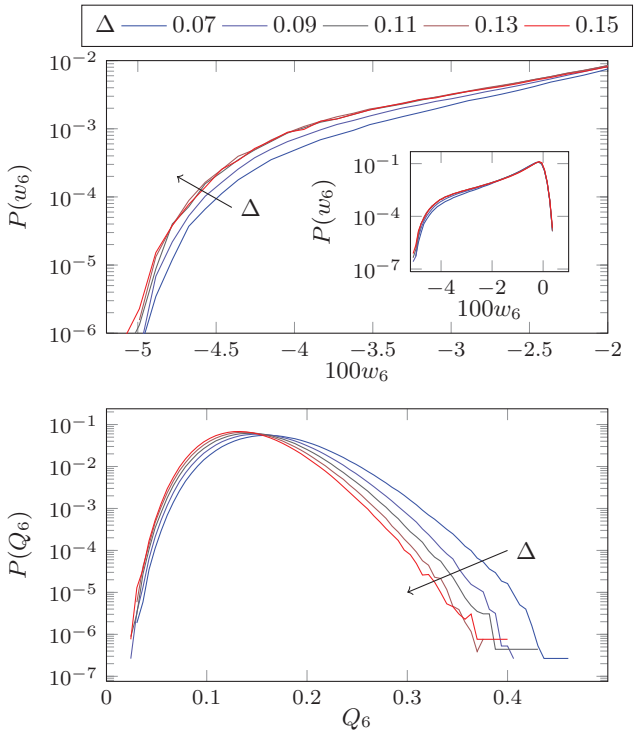

FIG. 7. Effect of polydispersity on local structures at constant pressure ($\beta p\sigma^3 = 23$): (top) detail of the distribution of w_6 (full distribution in inset) showing a small increase in the icosahedra population saturating around 10%; (bottom) distribution of Q_6 showing a marked decrease in the crystallinity with polydispersity.

correlation functions (not shown) of f_2 (respectively s_2) are perfectly identical at all pressures.

The choice of the threshold x^* is a balance between taking in too many particles or too few. If too few (below 5%), S_x is too noisy. If too many, the threshold does not discriminate between ordered and disordered particles and S_x tends to the trivial density $S(q)$. We found that between 5% and 40%, the absolute value of the length depends marginally on x^* but its pressure dependence does not. We chose to use 10% across this paper because this value allows the easiest direct visualization on a single frame (Fig. 6). We checked the pressure independence of the two-body parameter's length with thresholds up to 90%.

The study of correlation lengths has shown that by increasing pressure the range of crystal-like bond orientational order increases, driving the slowing down of the system as shown in Refs. 7 and 30. Bond orientational order corresponds to orientationally ordered regions which spontaneously form in the metastable phase. f_2 is instead decoupled from the relevant structures involved in the transition, as was shown in Fig. 3. We now address the question of how the system avoids crystallization despite the growing length-scale of bond orientational order.

C. Competition between icosahedral arrangements and crystal-like arrangements

We will now focus on the state point at $\beta p\sigma^3 = 23$ at different polydispersities to study the mechanism by which polydispersity disfavors the crystallization transition.

In Fig. 7 we show the probability distributions for the order parameters Q_6 and w_6 at different polydispersities. It is immediately evident that, while bond orientational order is rapidly suppressed with increasing polydispersity (as shown in the suppressed signal at high Q_6), particles in icosahedral environments are not disfavored by polydispersity. On the contrary, the fraction of icosahedral particles increases with polydispersity, and saturates at around $\Delta = 10\%$. This is in agreement with recent evidence of increased icosahedral ordering with size disparity in metallic glasses.[36] Intuitively, we can conclude that icosahedral order is more tolerant to size asymmetry (with the small particle usually sitting at the center of the icosahedral cage) than crystalline order is.

Figure 8 shows the metastable fluid distribution on the q_4-q_6 plane, which is a convenient representation as perfect icosahedral packings sit on the top-left corner of the distribution, while perfect crystals on the top-right corner. The figure clearly shows that, by increasing polydispersity, the biggest change in the metastable fluid distribution is the suppression

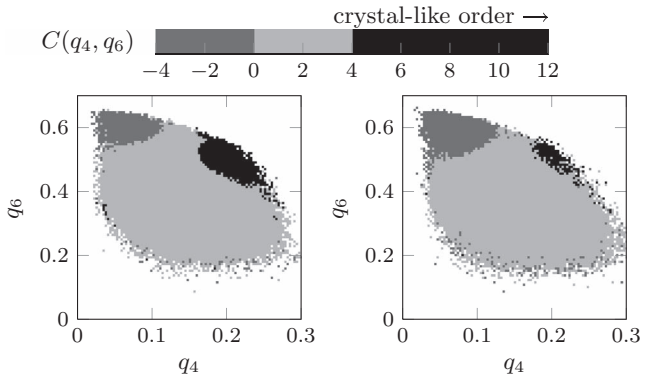

FIG. 8. Average crystallinity order parameter projected on the q_4-q_6 plane for the metastable fluid at $\beta p\sigma^3 = 23$ at $\Delta = 7\%$ (left) and $\Delta = 15\%$ (right). Icosahedra appear in the top-left corner of each plot (in dark gray) and perfect fcc crystals would be in the top-right corner with C = 12 (in black).

of crystal-like regions (high values of q_4, q_6, and C, the black region), while icosahedral environments are slightly enhanced (high q_6, low q_4, and negative C, the dark gray region).

The different effects of polydispersity on icosahedral and crystalline ordering are reflected in the different correlation lengths. Figure 9 shows the correlation length extracted from Q_6, w_6, and f_2 as a function of polydispersity. While the correlation length for Q_6 (associated with crystal-like regions) decreases with increasing polydispersity, the one extracted from w_6 (associated with icosahedral regions) increases. However, the two lengths are far from crossing and seem to saturate around $\Delta = 13\%$–15%. The correlation length of f_2 is constant or even slightly decreasing with Δ, never taking over the many-body lengths. It is thus clear that, in the present range of polydispersity, crystal-like bond order fluctuations are still the dominant contribution in the static (and dynamic[30]) properties of the system.

In Ref. 28 we have shown that the competition between crystalline packings and icosahedral packings can be studied via two-dimensional maps of translational vs orientational order. Orientational order is captured by q_6, which is small for disordered arrangement of particles and increases for both crystal-like and icosahedral particles. Translational order is instead measured with the local packing fraction, ϕ, obtained by measuring the volume of the Voronoi diagram associated with each particle. The calculation is straightforward:

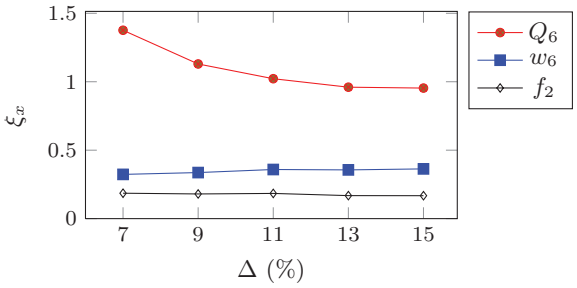

FIG. 9. Polydispersity dependence of the correlation lengths at $\beta p\sigma^3 = 23$. The dominant crystalline length decreases, the icosahedral length increases, however they plateau well before crossing. The two-body length shows no indication of becoming dominant with increasing Δ, even decreasing slightly.

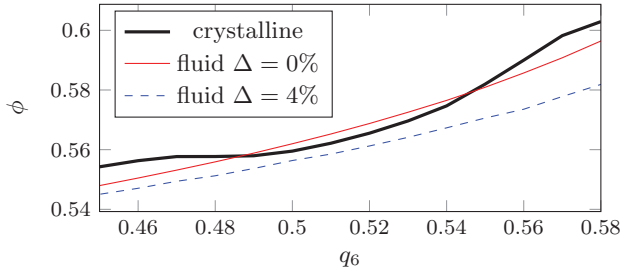

FIG. 10. Average ϕ as a function of q_6 for particles identified as "fluid" and "crystalline" according to the criteria outlined in Sec. II C. The continuous red curve represents fluid particles in a system at $\beta p\sigma^3 = 17$ and $\Delta = 0\%$, while dashed blue curve represents fluid particles at the same pressure but at $\Delta = 4\%$. The thick black curve represents instead crystalline particles (this curve is less sensitive to polydispersity and it is reported once). Note that, while in the monodisperse case there is a ϕ interval in which the crystalline particles have higher orientational order, in the polydisperse case crystalline particles have lower orientational order at all ϕ. While the monodisperse case is easily crystallized in direct simulations, the polydisperse system always remains metastable.

for each configuration, crystalline particles are identified with the method described in Sec. II C and the other particles are termed "fluid." For each subset of particles, the average value of the volume fraction ϕ is calculated as a function of the order parameter q_6, and plotted in Fig. 10. For each value of q_6 the map captures the average volume fraction ϕ of both crystalline and non-crystalline environments.

In Fig. 10 we compare the curves at $\beta p\sigma^3 = 17$ and at different polydispersities (see also the black diamonds of Fig. 1): at 0% (monodisperse system, red continuous curve) and at 4% (blue dashed curve). The curve for the crystalline particles is similar at the two considered polydispersities and is reported once as the thick solid line. First, we consider the monodisperse case. As shown in the figure, at low volume fraction, a particle in the fluid phase has higher orientational order than in the crystalline phase. But at $\phi \cong 55.8\%$, a crossover occurs and the crystal phase gains microscopic stability: a particle in a crystalline environment will have higher orientational order than a particle in the fluid phase at the same volume fraction. This crossover marks the appearance in the fluid phase of the metastable crystals which continuously appear, grow, and shrink, until eventually a crystal droplet reaches the critical size and starts the crystallization process. At a higher volume fraction ($\phi \cong 58\%$), another crossover occurs, with crystalline particles having less orientational order than particles in the "fluid" branch. These particles in the fluid phase at high q_6 are easily identified as particles in icosahedral packings (they have a low value of w_6). It is thus clear that icosahedral packings are competing with crystalline packings, eventually dominating at high ϕ. This scenario is confirmed by looking at the polydisperse case (blue dashed line in Fig. 10). At polydispersity $\Delta = 4\%$, the crystalline branch always lays above the fluid one, meaning that crystalline environments, at any fixed ϕ, are not able to attain higher bond orientational order than other configurations. Microscopically, the difference between the monodisperse and the polydisperse cases is due to an increased population of icosahedral particles, which dominate the fluid branch for $q_6 \gtrsim 0.5$. We have shown that, while for the monodisperse case there is a range of

volume fractions where crystalline particles attain higher orientational order than icosahedral arrangements, for the polydisperse case icosahedral particles always attain higher orientational order. This is immediately reflected in direct simulations, as at this pressure it is not possible to crystallize simulations at $\Delta = 4\%$, while the monodisperse simulations are easily crystallized.[37,38] Since the diffusional dynamics of the system, which controls the kinetic factor of crystallization,[39] is approximately the same at different values of Δ,[37] this difference in the crystallization behavior has to come from some structural difference introduced by polydispersity, i.e., an increased population of icosahedral particles (see Figs. 7 and 8). We also confirm that at polydispersity $\Delta = 7\%$, icosahedral particles are favored over crystalline ones for all the pressures studied, in line with the observation of Fasolo and Sollich[40] that one-phase crystallization is suppressed at high polydispersity.

We have thus provided direct evidence that icosahedral particles are responsible for the suppression of crystallization in polydisperse hard spheres.

IV. DISCUSSION

In the present study we have compared the evolution of static length-scales in polydisperse hard spheres for both two-body and many-body correlation functions. While two-body correlation functions do not show any sign of an increasing length-scale with pressure, we have confirmed that in the glass transition of polydisperse hard spheres the relevant static length is the correlation length of the crystal-like bond order. We have also determined the relevant microscopic structures that are associated with the increasing length-scale: they correspond to crystal-like environments of particles and are characterized by slow dynamics. We thus confirm that in the glass transition of polydisperse hard spheres, the relevant static length is the correlation length of the crystal-like bond orientational order.

The other relevant structure with slow dynamics is icosahedral packings of particles, but its length-scale does not grow appreciably with increasing pressure. Icosahedral assemblies of particles are spatially uncorrelated. While not having a direct role in the slowing down of the dynamics, we have shown that icosahedral packings are responsible for the avoidance of the crystallization transition with increasing polydispersity. The increase in polydispersity reduces the degree of crystal-like bond orientational order, whereas enhances the icosahedral order (see Figs. 7 and 8). The former is crucial for triggering crystal nucleation,[28] whereas the latter leads to the frustration against crystallization, a role that increases with polydispersity. None of these physical aspects of the system could be described by two-body quantities.

We previously showed that spatial fluctuations of crystal-like bond orientational order are closely correlated with local dynamics: more ordered regions have slower dynamics.[7,30,41–44] Together with these results, we may say that it is many-body correlations, or crystal-like bond orientational ordering, that are the cause of slow dynamics and dynamic heterogeneity. This means that future theories of glass transition and crystallization should deal with many-body correlation effects properly. The link between the symmetry of the relevant bond order parameter for describing structural ordering in a supercooled liquid and that for crystallization is another interesting point. This may be a direct consequence of the fact that glass transition is governed by the same free energy as that controlling crystallization.[45–47] This conjecture is further supported by the role of polydispersity in the glass-forming ability of hard spheres.

The mechanism by which polydispersity increases the barrier for crystal nucleation may be twofold: (i) direct random disorder effect which destroys crystal-like bond orientational order in a supercooled liquid, which is the first step in crystal nucleation;[28] (ii) enhancement of icosahedral ordering with an increase in the polydispersity. It is known that size disparity between a particle and its surrounding neighbors stabilizes icosahedral order.[36] Since the symmetry of icosahedral order is not consistent with that of the equilibrium crystal polymorphs (fcc and hcp for this case), competing ordering toward these two mutually inconsistent symmetries leads to strong frustration effects on crystallization, as in the case of 2D spin liquids.[43,48] The results shown in Fig. 10 suggest that mechanism (ii) may be more relevant for the suppression of crystallization.

Although we studied polydisperse hard spheres in this article, these frustration mechanisms should be relevant to many other glass-forming systems including metallic glass formers.[9,49]

V. SUMMARY

In this article, we show firm evidence for the importance of many-body correlations in glass transition phenomena for hard spheres liquids. This feature cannot be described by the standard liquid-state theories based on two-body correlation. In relation to this, we note that Berthier and Tarjus recently questioned the validity of "microscopic" approaches to the slow dynamics of glass-forming liquids based on the sole knowledge of the static pair density correlations.[50] We argue that, at high density, liquid state packing effects inevitably lead to many-body correlations, which play key roles in phenomena like the glass transition and crystallization. A physically natural order parameter to pick up these many-body correlations is the *bond order parameter*, whose importance has been well recognized and established for ordering transitions of hard disks in 2D.[51] We believe in the importance of incorporating many-body correlations into theories to describe both the glass transition and crystallization phenomena properly.[46,47]

Our study also indicates that there is an intrinsic link between crystallization and vitrification. Whether a polydisperse hard spheres system is crystallized or vitrified can be controlled just by changing polydispersity, which affects extendable crystal-like bond orientational order and isolated icosahedral order in an opposite manner. We speculate that this direct link may exist for systems where crystallization does not involve phase separation, in other words, as far as the two phenomena are described by the same free energy.[45–47] How universal is this scenario needs to be checked carefully in the future.

ACKNOWLEDGMENTS

The authors are grateful to Daniel Bonn for fruitful discussion and drawing our attention to Ref. 25. This study was partly supported by a grant-in-aid from the Ministry of Education, Culture, Sports, Science and Technology, Japan (Kakenhi) and by the Japan Society for the Promotion of Science (JSPS) through its "Funding Program for World-Leading Innovative R&D on Science and Technology (FIRST Program)" and a JSPS Postdoctoral Fellowship.

[1] S. Petit and G. Coquerel, in *Polymorphism: In the Pharmaceutical Industry* (Wiley-VCH, 2006), pp. 259–285.
[2] K. Grzybowska, M. Paluch, P. Wlodarczyk, A. Grzybowski, K. Kaminski, L. Hawelek, D. Zakowiecki, A. Kasprzycka, and I. Jankowska-Sumara, Mol. Pharmacol. **9**, 894 (2012).
[3] A. Cavagna, Phys. Rep. **476**, 51 (2009).
[4] L. Berthier and G. Biroli, Rev. Mod. Phys. **83**, 587 (2011).
[5] R. Yamamoto and A. Onuki, Phys. Rev. E **58**, 3515 (1998).
[6] C. Donati, S. C. Glotzer, P. H. Poole, W. Kob, and S. J. Plimpton, Phys. Rev. E **60**, 3107 (1999).
[7] H. Tanaka, T. Kawasaki, H. Shintani, and K. Watanabe, Nature Mater. **9**, 324 (2010).
[8] M. M. J. Treacy and K. B. Borisenko, Science **335**, 950 (2012).
[9] J. Hwang, Z. Melgarejo, Y. Kalay, I. Kalay, M. Kramer, D. Stone, and P. Voyles, Phys. Rev. Lett. **108**, 195505 (2012).
[10] V. Lubchenko and P. G. Wolynes, Annu. Rev. Phys. Chem. **58**, 235 (2007).
[11] G. Biroli, J. P. Bouchaud, A. Cavagna, T. S. Grigera, and P. Verrocchio, Nat. Phys. **4**, 771 (2008).
[12] G. Parisi and F. Zamponi, Rev. Mod. Phys. **82**, 789 (2010).
[13] M. Fasolo and P. Sollich, Phys. Rev. Lett. **91**, 068301 (2003).
[14] A. Hopkins, Y. Jiao, F. Stillinger, and S. Torquato, Phys. Rev. Lett. **107**, 125501 (2011).
[15] A. Hopkins, F. Stillinger, and S. Torquato, Phys. Rev. E **85**, 021130 (2012).
[16] B. Charbonneau, P. Charbonneau, and G. Tarjus, Phys. Rev. Lett. **108**, 035701 (2012).
[17] D. Coslovich, Phys. Rev. E **83**, 051505 (2011).
[18] A. Malins, J. Eggers, C. P. Royall, S. R. Williams, and H. Tanaka, J. Chem. Phys. **138**, 12A535 (2013).
[19] M. Mosayebi, E. Del Gado, P. Ilg, and H. C. Öttinger, Phys. Rev. Lett. **104**, 205704 (2010).
[20] M. Mosayebi, E. Del Gado, P. Ilg, and H. C. Öttinger, J. Chem. Phys. **137**, 024504 (2012).
[21] R. E. Nettleton and M. S. Green, J. Chem. Phys. **29**, 1365 (1958).
[22] R. D. Mountain, J. Chem. Phys. **55**, 2250 (1971).
[23] K. Watanabe, T. Kawasaki, and H. Tanaka, Nature Mater. **10**, 512 (2011).
[24] T. Kawasaki and H. Tanaka, J. Phys.: Condens. Matter **23**, 194121 (2011).
[25] T. Aste and A. Coniglio, EPL **67**, 165 (2004).
[26] P. J. Steinhardt, D. R. Nelson, and M. Ronchetti, Phys. Rev. B **28**, 784 (1983).
[27] S. Auer and D. Frenkel, J. Chem. Phys. **120**, 3015 (2004).
[28] J. Russo and H. Tanaka, Sci. Rep. **2**, 505 (2012).
[29] W. Lechner and C. Dellago, J. Chem. Phys. **129**, 114707 (2008).
[30] M. Leocmach and H. Tanaka, Nat. Commun. **3**, 974 (2012).
[31] S. Kapfer, W. Mickel, K. Mecke, and G. Schröder-Turk, Phys. Rev. E **85**, 030301 (2012).
[32] T. Kawasaki and H. Tanaka, Proc. Natl. Acad. Sci. U.S.A. **107**, 14036 (2010).
[33] J. Russo and H. Tanaka, Soft Matter **8**, 4206 (2012).
[34] E. Flenner, M. Zhang, and G. Szamel, Phys. Rev. E **83**, 051501 (2011).
[35] Please note that the calculation in Fourier space is done here by retaining the 10% most ordered particles for each order parameter. For q_6 this means collecting the signal almost entirely from icosahedral particles. A real space analysis, done by including all particles, shows instead that the correlation length of the tensorial q_{6m} is increasing as it discards the correlation between icosahedra of incoherent orientations, keeping only bond-orientational ordered structures.
[36] M. Shimono and H. Onodera, Rev. Metall./Cah. Inf. Tech. **109**, 41 (2012).
[37] E. Zaccarelli, C. Valeriani, E. Sanz, W. C. K. Poon, M. E. Cates, and P. N. Pusey, Phys. Rev. Lett. **103**, 135704 (2009).
[38] P. Pusey, E. Zaccarelli, C. Valeriani, E. Sanz, W. Poon, and M. Cates, Philos. Trans. R. Soc. London, Ser. A **367**, 4993 (2009).
[39] H. Tanaka, Phys. Rev. E **68**, 011505 (2003).
[40] M. Fasolo and P. Sollich, Phys. Rev. E **70**, 041410 (2004).
[41] T. Kawasaki, T. Araki, and H. Tanaka, Phys. Rev. Lett. **99**, 215701 (2007).
[42] K. Watanabe and H. Tanaka, Phys. Rev. Lett. **100**, 158002 (2008).
[43] H. Shintani and H. Tanaka, Nat. Phys. **2**, 200 (2006).
[44] T. Kawasaki and H. Tanaka, J. Phys.: Condens. Matter **22**, 232102 (2010).
[45] H. Tanaka, J. Phys.: Condens. Matter **10**, L207 (1998).
[46] H. Tanaka, J. Stat. Mech.: Theory Exp. **2010**, P12001 (2010).
[47] H. Tanaka, Eur. Phys. J. E **35**, 113 (2012).
[48] H. Shintani and H. Tanaka, Nature Mater. **7**, 870 (2008).
[49] N. Jakse and A. Pasturel, Phys. Rev. B **78**, 214204 (2008).
[50] L. Berthier and G. Tarjus, Eur. Phys. J. E **34**, 96 (2011).
[51] D. R. Nelson, *Defects and Geometry in Condensed Matter Physics* (Cambridge University Press, Cambridge, 2002).